Gao *et al. Cell & Bioscience* (2026) 16:61
https://doi.org/10.1186/s13578-026-01599-8

Cell & Bioscience

RESEARCH Open Access

lncRNA-operated stem cell fate control: RPS3 mediates the in situ *Gm16751–Zhx3* interactome to program spermatogonial stem cell differentiation

Weijun Gao[1], Bo Xu[2], Wenzhi Ma[1], Xiaojin He[3,4] and Ji Wu[1,2*]

Abstract

Background Long non-coding RNAs (lncRNAs) play pivotal regulatory roles in mammalian male gametogenesis. Advances in high-throughput technologies have demonstrated that lncRNAs orchestrate robust, flexible, and context-specific gene regulatory networks through dynamic interactions with proteins, DNA, and RNA, modulating transcriptional and post-transcriptional processes. However, the mechanistic role of in situ lncRNA-mRNA interactions in spermatogonial stem cell (SSC) differentiation remains poorly understood.

Methods The differentially expressed transcripts, including lncRNA, mRNA and circRNA, were systematically identified through long RNA sequencing (LongRNA-seq). RNA-RNA in situ interactions were subsequently mapped using RNA in situ conformation sequencing (RIC-seq) technology. The *Gm16751–Zhx3* interaction was validated using single-molecule fluorescence in situ hybridization (smFISH), coupled with RNA antisense purification followed by quantitative PCR (RAP-qPCR), and dual-luciferase reporter assay. Its functional impact on SSC differentiation was assessed via EdU staining, apoptosis assay, mRNA stability assay, RAP-qPCR, respectively. Liquid chromatography-tandem mass spectrometry (LC-MS) and RNA immunoprecipitation-qPCR (RIP-qPCR) were employed to screen and identify the RNA-binding protein (RBP) interacting with *Gm16751* and *Zhx3*. Crosslinking immunoprecipitation followed by qPCR (CLIP-qPCR) further identified specific binding sequences. The regulation of RBP on the differentiation of SSC was verified using RAP-qPCR, RIP-qPCR, puromycin incorporation assay, and RNA stability assay.

Results We employed RIC-seq and LongRNA-seq to systematically identify a functional interaction between lncRNA *Gm16751* and *Zhx3* mRNA during SSC differentiation, which was further visualized via a Circos plot. Mechanistically, we demonstrated that *Gm16751* enhances the mRNA stability of *Zhx3*, thereby promoting SSC differentiation. Furthermore, mass spectrometry analysis revealed that RPS3 (Ribosomal Protein S3) serves as a critical RBP that bridges the interaction between *Gm16751* and *Zhx3*, ultimately stabilizing *Zhx3* mRNA and modulating SSC differentiation.

*Correspondence:
Ji Wu
jiwu@sjtu.edu.cn

Full list of author information is available at the end of the article

Conclusions Our study identified a novel lncRNA-mRNA interaction pair, *Gm16751/Zhx3*, which is mediated by RPS3 and facilitates the differentiation of SSC. This discovery provides important mechanistic insights into the regulation of male germ cell development and offers a new perspective for understanding molecular controls in spermatogenesis.

Keywords lncRNA, RIC-seq, RNA in situ interaction, RBP, SSC

Graphical abstract

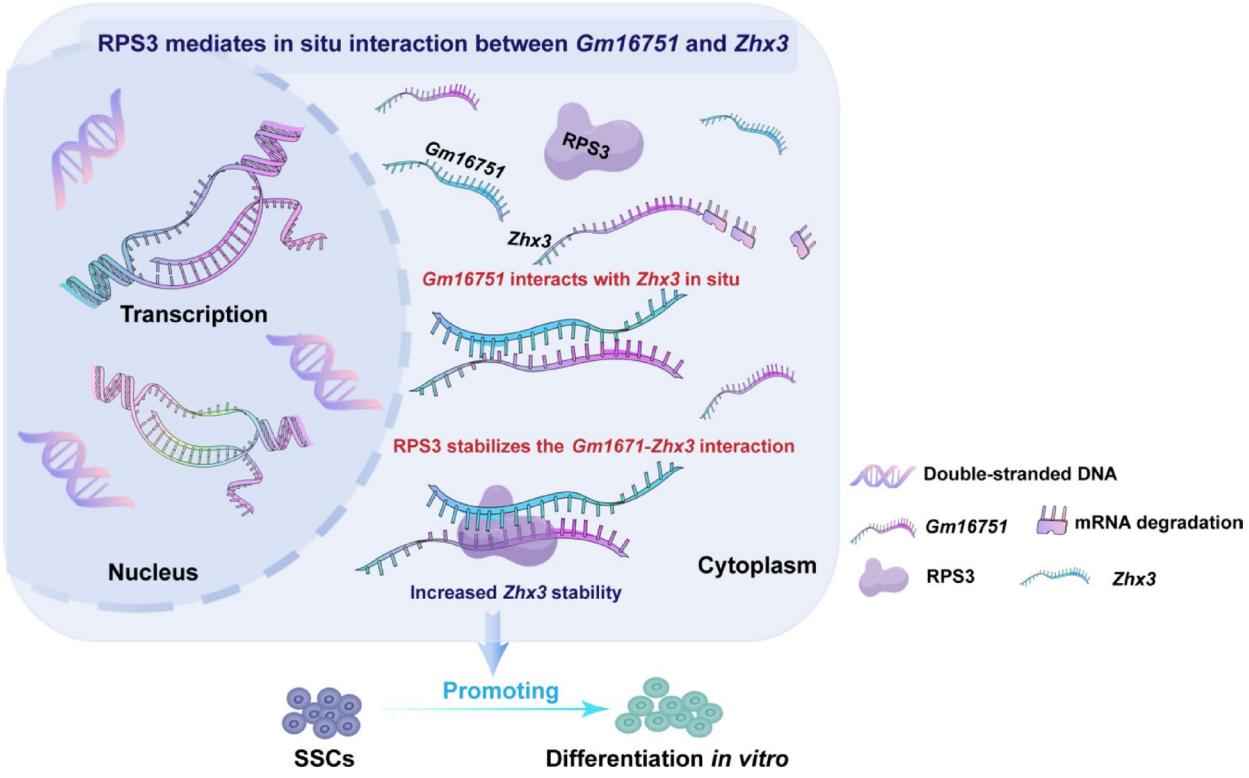

Introduction

Long non-coding RNAs (lncRNAs), defined as non-coding transcripts exceeding 200 nucleotides, are ubiquitously expressed in eukaryotes and far outnumber protein-coding mRNAs [1]. This diverse class includes enhancer-associated lncRNAs (elncRNAs), promoter-interacting lncRNAs, and antisense lncRNAs, among others, which play critical roles in gene regulation [2]. High-throughput sequencing has revealed that lncRNAs establish dynamic, context-specific regulatory networks by interacting with proteins, DNA, and RNA to modulate transcriptional and post-transcriptional processes [2, 3].

In mammalian male gametogenesis, lncRNAs serve as essential regulators. For instance, ACVR2B-as1 interacts with ALDOA to control glycolysis, thereby regulating self-renewal and apoptosis in human spermatogonial stem cells (SSCs) [4]. *Mrhl* lncRNA modulates meiotic progression by binding the *Sox8* promoter and influencing Wnt signaling [5]. And the lncRNA *Gm2044* is highly expressed in spermatocytes, where it suppresses *Utf1* mRNA translation through interaction, plays a critical role in regulating spermatogenesis [6]. lncRNAs also contribute to epigenetic regulation, such as X chromosome inactivation during early female embryogenesis [3, 7, 8]. Previous studies have detected *Gm16751* expression in adult mouse testis [9], its functional role and regulatory mechanism within the SSC differentiation pathway remain entirely unexplored. The regulatory functions of lncRNAs are closely linked to their subcellular localization. Nuclear lncRNAs govern chromatin remodeling, RNA splicing, and transcriptional regulation. Cytoplasmic lncRNAs regulate mRNA transport, stability, and translation [10, 11]. Moreover, their activity often depends on interactions with RNA-binding proteins (RBPs), which serve as critical mediators of lncRNAs function [2].

RBPs selectively bind RNA to form ribonucleoprotein (RNP) complexes, acting as key post-transcriptional regulators [12]. lncRNAs can scaffold RBPs to specific genomic loci, modulating cis- and trans-regulatory networks [13, 14]. Emerging evidence highlights that lncRNA-RBP interactions regulate mRNA stability, a

mechanism implicated in tumorigenesis and gametogenesis [15–17]. Notably, RBPs are indispensable for spermatogenesis. DDX20, a conserved DEAD-box helicase, controls progenitor spermatogonia formation and SSC pool maintenance by regulating cell cycle-related mRNA translation [18]. In *C. elegans*, the AMG-1/SLRP-1 RBP complex sustains spermatogenesis by maintaining mitochondrial homeostasis [19]. These findings underscore the biological significance of RBP-lncRNA-mRNA networks in male germline development. Normal spermatogenesis relies on a tightly regulated balance between SSC self-renewal and differentiation [20, 21]. While numerous lncRNAs have been identified via high-throughput sequencing, their functional mechanisms, particularly how RBPs mediate lncRNA-mRNA interactions in SSC differentiation, remain poorly understood. Recent advances in RNA structural biology reveal that RNAs with complex conformations often form multi-RBP complexes, orchestrating critical biological pathways [22]. RNA in situ conformation sequencing (RIC-seq) enables in situ mapping of RNA-RNA interactions mediated by RBPs, providing unprecedented insights into lncRNA-mRNA regulatory networks [22].

Using LongRNA-seq and RIC-seq, we identified 2,194 differentially interacting lncRNA-mRNA pairs during SSC differentiation. Among these, the *Gm16751–Zhx3* interaction was significantly upregulated upon differentiation. Mechanistically, *Gm16751* enhances *Zhx3* mRNA stability, promoting SSC differentiation. Mass spectrometry revealed RPS3 (Ribosomal Protein S3) as an RBP that binds *Gm16751*. RPS3 mediates the *Gm16751–Zhx3* interaction, further stabilizing *Zhx3* mRNA and driving differentiation. This study elucidates a novel lncRNA-RBP-mRNA regulatory axis in SSC differentiation, offering critical insights into male germ cell development disorders and infertility mechanisms.

Materials and methods

Animals

ICR mice were obtained from Shanghai SLAC Laboratory Animal Co. Ltd. All animal procedures were approved by the Shanghai Animal Care and Utilization Committee and conducted in compliance with the National Research Council's Guidelines for the Care and Use of Laboratory Animals. Six-week-old male and female mice were housed at a 1:1 ratio, and testes from 6-day-old F1 male pups were used for experiments. The ethics approval number is A2023127-001.

Isolation and culture of mouse spermatogonial stem cells (mSSCs)

mSSCs were isolated and cultured as previously described [23]. Briefly, testes from 6-day-old postnatal mice were dissociated via a two-step enzymatic digestion. SSCs were purified using anti-mouse CD90.2 magnetic beads and seeded onto mitomycin C-treated STO or mouse embryonic fibroblast (MEF) feeder layers in 48- or 24-well plates. Cultures were maintained at 37 °C with 5% CO_2. Half of the medium was replaced daily, and cells were passaged at a 1:2 ratio every 6–7 days.

Retinoic acid induces SSC differentiation into meiosis

Sertoli cells from 6-day-old mice were isolated and cultured to prepare feeder layers [24]. mSSCs grown on MEF feeders were dissociated with 0.05% trypsin (1 min), then transferred onto Sertoli cell feeders in differentiation medium supplemented with 2 μM retinoic acid for 3 days. The differentiation medium consisted of MEM-α, 10% FBS, 100 IU/mL penicillin, 100 μg/mL streptomycin, 1× vitamins, 1 mM non-essential amino acids, 10 ng/mL GDNF, 10 ng/mL EGF, 20 ng/mL bFGF, 10 ng/mL LIF, 0.1 mM β-mercaptoethanol, 25 μg/mL insulin, 100 μg/mL human transferrin, 60 μM putrescine, 1 mM sodium pyruvate, 60 ng/mL progesterone, and 2 mM L-glutamine.

RT-PCR and qRT-PCR

Total RNA was extracted using TRIzol reagent, and cDNA was synthesized following manufacturer protocols. RT-PCR and qRT-PCR were performed using primers listed in Supplementary Table 1.

Immunofluorescence staining

Cells were washed with PBS, fixed in 4% paraformaldehyde (15–20 min, RT), and permeabilized with 0.5% Triton X-100 (20 min; omitted for membrane proteins like MVH). After blocking with 10% goat serum (37 °C, 20–30 min), primary antibodies (1:100-1:200) were applied overnight at 4 °C. Alexa Fluor 488/594-conjugated secondary antibodies (1:200) were incubated for 1 h at RT. Nuclei were counterstained with DAPI, and images were acquired using a Leica DMI3000B fluorescence microscope. Antibody details were provided in Supplementary Table 2.

Western blotting

Cells were lysed in RIPA buffer with protease inhibitors, and protein concentrations were determined via BCA assay (YEASEN). Proteins were separated on 10% SDS-PAGE gels, transferred to PVDF membranes, and blocked with 5% skim milk. Primary antibodies were incubated overnight at 4 °C, followed by HRP-conjugated secondary antibodies (1 h, RT). Blots were visualized using ECL reagent (VILBER), and band intensities were quantified with ImageJ. Antibodies were listed in Supplementary Table 2.

Long RNA sequencing (LongRNA-seq)

Total RNA was extracted with TRIzol, and RNA quality was verified by 1% agarose gel electrophoresis. And rRNA-depleted libraries were prepared using the Epi™ Mini LongRNA-seq Kit (Guangzhou Epibiotek). Library quality was assessed using the Bioptic Qsep100 Analyzer. Paired-end sequencing (150 bp) was performed on a NovaSeq 6000. Clean reads were aligned to the reference genome using HISAT2.

RNA in situ conformation sequencing (RIC-seq)

Cells were crosslinked with 1% formaldehyde (10 min, RT), washed the cells once with pre-cooled 1× PBS, and added glycine buffer to terminate crosslinked. Collected the cell pellet and rapidly freeze it with liquid nitrogen (more than 30s). Chimeric reads were enriched as described [22], and sequenced on an Illumina HiSeq X Ten. Data were analyzed using STAR (v2.2.0.1).

Single-molecule fluorescence in situ hybridization (smFISH)

Probes targeting *Gm16751* (Cy3) and *Zhx3* (Cy5) (GenePharma) were hybridized using the smFISH Assay Kit (GenePharma, F50111). Cells were fixed in 4% PFA (15 min, RT), and probes were denatured (65 °C, 3 min) before hybridization (37 °C, 12–16 h). Amplification and imager probes were sequentially applied, and nuclei were stained with DAPI. Images were captured using a STELLARIS 5 confocal microscope, and fluorescence intensities were quantified with ImageJ. The smFISH probe sequences were listed in Supplementary Table 3.

RNA antisense purification (RAP) and lncRNA knockdown

Gm16751-specific RAP probes (BersinBio) were used with the RNA Antisense Purification Kit (Bes5103-2) [25]. For knockdown, cells were transfected with 50 pmol locked nucleic acid (LNA) antisense oligonucleotides (ASOs) (Guangzhou Epibiotek) for 48 h [22], followed by qRT-PCR validation. The RAP probe sequences and LNA ASO sequences were listed in Supplementary Table 4, Tables 7, and Table 5, respectively.

Dual-luciferase reporter assay

3T3 cells were seeded in 24-well plates and cultured for 24 h prior to transfection with plasmid using Lipo8000 transfection reagent (Beyotime, C0533). The wild-type pmirGLO-*Gm16751* reporter or its mutant version (pmirGLO-*Gm16751*-mut) reporter vector was co-transfected into 3T3 cells with pcDNA3.1–*Zhx3* 3′UTR and pRL-TK plasmid. Firefly luciferase activity was quantified using the Dual Luciferase Reporter Gene Assay Kit (Yeasen, 11402ES60) and normalized to corresponding Renilla luciferase internal controls. The primer sequences for plasmid construction were listed in Supplementary Table 6.

mRNA stability assay

Cells treated with LNA ASO or *shRps3* were exposed to 80 μM DRB for 0–3 h. Cells were harvested at 0, 1, 2, and 3 h post-DRB treatment, and total RNA was extracted from each time point using TRIzol reagent. The expression level of *Zhx3* mRNA was then analyzed by qRT-PCR and normalized to the 0 h timepoint to determine the decay curve and calculate the half-life ($t_{1/2}$).

RNA immunoprecipitation (RIP)-qPCR

RIP was performed using the PureBinding® RIP Kit (GENESEED, P0102). Lysates were incubated with protein A/G beads conjugated to anti-RPS3 or IgG (5 μg, 4 °C overnight). Precipitated RNA was analyzed by qRT-PCR for *Gm16751* and *Zhx3*.

Crosslinking immunoprecipitation-qPCR (CLIP-qPCR)

Using the crosslinking immunoprecipitation and qPCR Kit from BersinBio (Bes3014-1), a CLIP assay was performed according to the manufacturer's instructions to identify the specific *Gm16751* and *Zhx3* sequences bind to RPS3. Cells were treated with 100 μM 4-thiouridine (Sigma, T4509) for 16 h, followed by ultraviolet light cross-linking at 365 nm for 10 min. RPS3 antibody was added to the cell lysate to capture RPS3-RNA complexes, and collected the RNA. The immunoprecipitated RNA was subsequently subjected to tailing reverse transcription and qPCR analysis. The CLIP-qPCR primer sequences were listed in Supplementary Table 7.

Puromycin incorporation assay

Cells were treated with 5 μg/mL puromycin (1 h), and lysates were immunoblotted with anti-puromycin (1:2000, ABclonal, A21205) or stained with Coomassie blue.

EdU staining

Proliferation was assessed using the Cell-Light EdU Apollo567 Kit (RiboBio, C10310-1). Images were acquired on a Leica DMI3000B, and EdU^+ cells were quantified with ImageJ.

Apoptosis assay

Cells ($1–10 \times 10^5$) were stained with Annexin V-APC/PE (absin, abs50008) and analyzed by flow cytometry (Beckman Coulter). Data were processed using FlowJo (v10.9.0).

Statistical analysis

Data from three independent experiments were presented as mean ± SEM. Comparisons between two groups

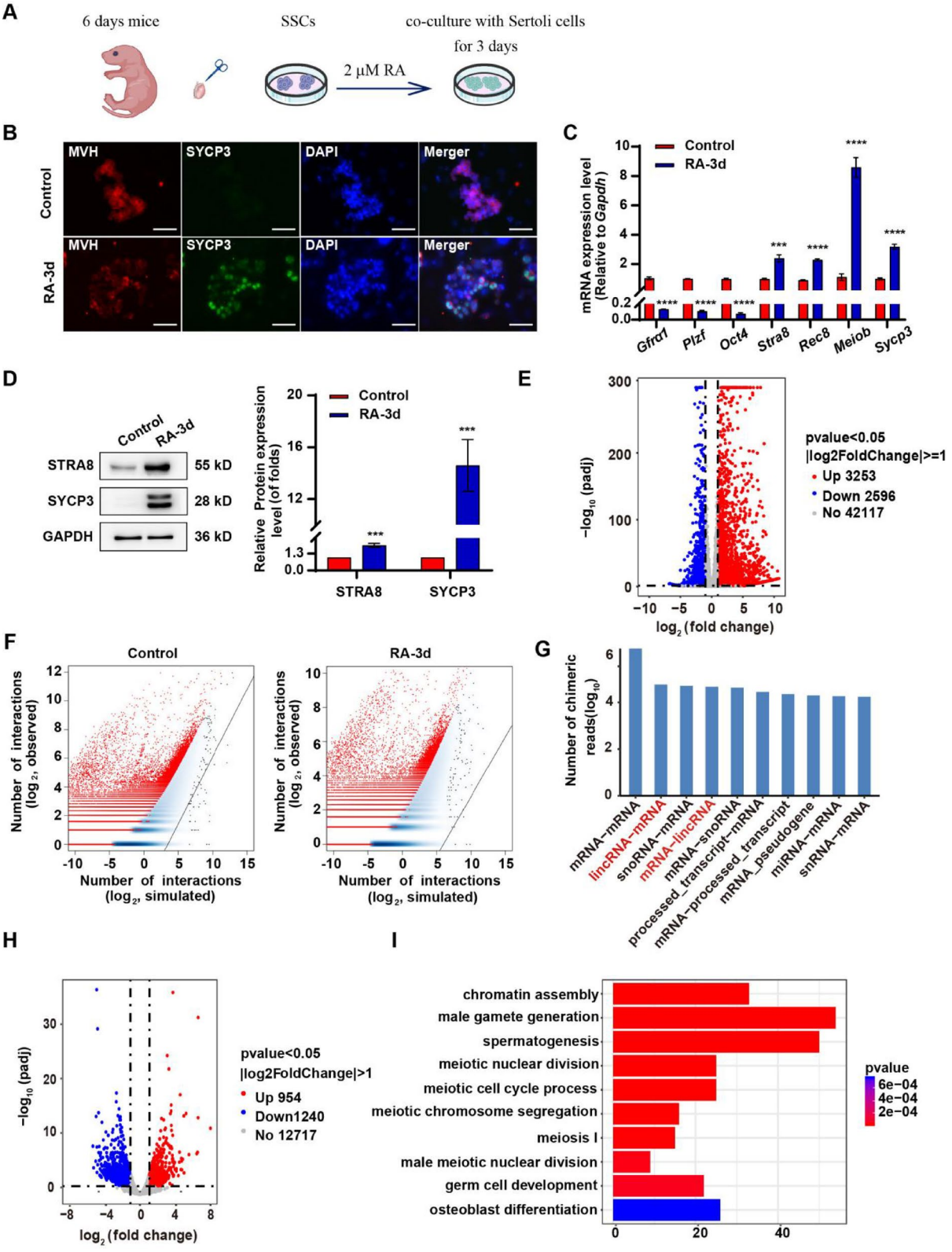

Fig. 1 (See legend on next page.)

(See figure on previous page.)

Fig. 1 LongRNA-seq and RIC-seq profiling of transcriptome dynamics and RNA interactome during SSC differentiation. **A** Schematic of the SSC differentiation protocol. **B** SYCP3 immunofluorescence staining on day 3 of RA-induced differentiation, demonstrating meiotic progression (Control: Undifferentiated spermatogonia stem cells, the same below). **C** qRT-PCR analysis of *Plzf*, *Gfra1*, *Oct4*, *Stra8*, *Rec8*, *Meiob* and *Sycp3* expression during SSC differentiation. **D** Western blotting analysis of STRA8 and SYCP3 protein levels. **E** Volcano plot of differentially expressed RNAs (lncRNAs, mRNAs, and circRNAs). **F** This scatter plot visualizes the distribution of RNA-RNA interaction reads between the observed and expected. Interactions with observed significantly higher than the predicted background levels (red points) are classified as high-confidence, the sloped line represents a linear fit. **G** Classification of interaction read types (e.g., lncRNA-mRNA). **H** Volcano plot of differentially interacting RNA pairs. **I** GO enrichment analysis of RNAs with altered interaction patterns. Data represent mean ± SEM. $n = 3$ independent repeats. Scale bar: 50 μm. Statistical significance: ***$P < 0.001$, ****$P < 0.0001$

used unpaired *t*-tests; multiple groups were analyzed by one-way ANOVA ($P < 0.05$). Graphs were generated with GraphPad Prism 9.

Results

LongRNA-seq and RIC-seq analysis reveals transcriptome dynamics and RNA interactome remodeling during SSC differentiation

SSCs were isolated from 6-day-old ICR male mice using a two-step enzymatic digestion followed by CD90.2 magnetic bead purification. The cells were then cultured short-term on MEF feeder layers (Fig. S1A). SSC identity was confirmed through RT-PCR and immunostaining, which revealed expression of key self-renewal markers (*Plzf*, *Gfrα1*, *Etv5*, and *Oct4*) and the germ cell-specific marker *Mvh* (Fig. S1B). Immunofluorescence staining indicated nuclear localization of both PLZF and OCT4, in addition to positive expression of MVH and GFRα1 (Fig. S1C).

To establish an in vitro differentiation system, SSCs were co-cultured with Sertoli cells from 6-day-old mice in medium containing 2 μM retinoic acid (RA) [24]. After 3 days of induction, we observed the induced germ cells were in the form of monolayer patches with weak or strong SYCP3 immunostaining (Fig. 1A-B). qRT-PCR analysis revealed significant downregulation of *Plzf*, *Gfrα1* and *Oct4* concurrent with upregulation of meiotic markers (*Stra8*, *Rec8*, *Meiob*, *Sycp3*) (Fig. 1C). Western blotting confirmed increased protein expression of STRA8 and SYCP3 following induction (Fig. 1D). To visually track meiotic progression, we developed a CMV-mCherry-*Sycp3* promoter-eGFP dual-reporter lentiviral vector (Fig. S1D-H). Successful differentiation was evidenced by eGFP expression in SSCs after 3 days of 2 μM RA treatment (Supplementary Table 8, Fig. S1I). These results demonstrate that the isolated cells possess characteristic SSC properties and can be efficiently induced into meiosis using 2 μM RA.

To investigate transcriptomic changes and in situ RNA-RNA interactions during SSC differentiation, we performed LongRNA-seq and RIC-seq analyses on undifferentiated SSC and their differentiated counterparts. LongRNA-seq identified 5,849 differentially expressed genes (DEGs), including 1,303 lncRNAs, 4,441 mRNAs, and 106 circRNAs (Fig. 1E and Fig. S2A-B). Among the differentially expressed mRNAs, key SSC differentiation markers such as *Sycp1*, *Sycp2*, *Sycp3*, *Meiob*, and *Meioc* were significantly upregulated (Fig. S2D). Gene Ontology (GO) enrichment analysis of the DEGs revealed that upregulated mRNAs were predominantly associated with biological processes critical for differentiation, including male gametogenesis, germ cell development, and meiosis (Fig. S2C).

To map global RNA-RNA interactions in situ, we conducted RIC-seq and captured numerous chimeric reads in both groups (Fig. S2E-F and Supplementary Table 9). These chimeric reads yielded highly reproducible interaction profiles between the two groups (Fig. 1F), and encompassed diverse interaction types, including lncRNA-mRNA interactions (Fig. 1G). Integrating RIC-seq with LongRNA-seq data, we identified 2,194 differentially interacting RNAs during SSC differentiation (Fig. 1H). GO analysis of upregulated interactions further highlighted enrichment in terms related to male gametogenesis, meiosis, and germ cell development (Fig. 1I). Additionally, we detected multiple hubRNAs exhibiting extensive interaction networks (Fig. S2G-H), suggesting their potential regulatory roles. Together, these findings underscore widespread alterations in RNA expression and interactome dynamics during SSC differentiation.

Interaction between lncRNA *Gm16751* and mRNA *Zhx3* regulates SSC differentiation

To investigate the role of RNA-RNA interactions in SSC differentiation, we systematically analyzed the interaction sequencing data following SSC differentiation. After excluding interactions between identical RNAs, pseudogene-mRNA pairs, and intra-class RNA interactions, we identified significantly upregulated lncRNA-mRNA interaction pairs during SSC differentiation, specifically selecting those pairs where both partners showed co-upregulation. Through this screening, we ultimately validated a functional interaction between lncRNA *Gm16751* and mRNA *Zhx3*. They are all genes located on the reverse strand of chromosome 2 (GRCm38.91 or Ensembl GRCm38.p3, *Gm16751*: chromosome 2: 160840836–160888028; *Zhx3*: chromosome 2: 160,748,708–160,872,998). Moreover, we captured and presented chimeric reads that show the interaction between *Gm16751* and *Zhx3* (Supplementary Table 9). Although the circos plot analysis revealed that *Gm16751* interacts with multiple genes, and the overall number of

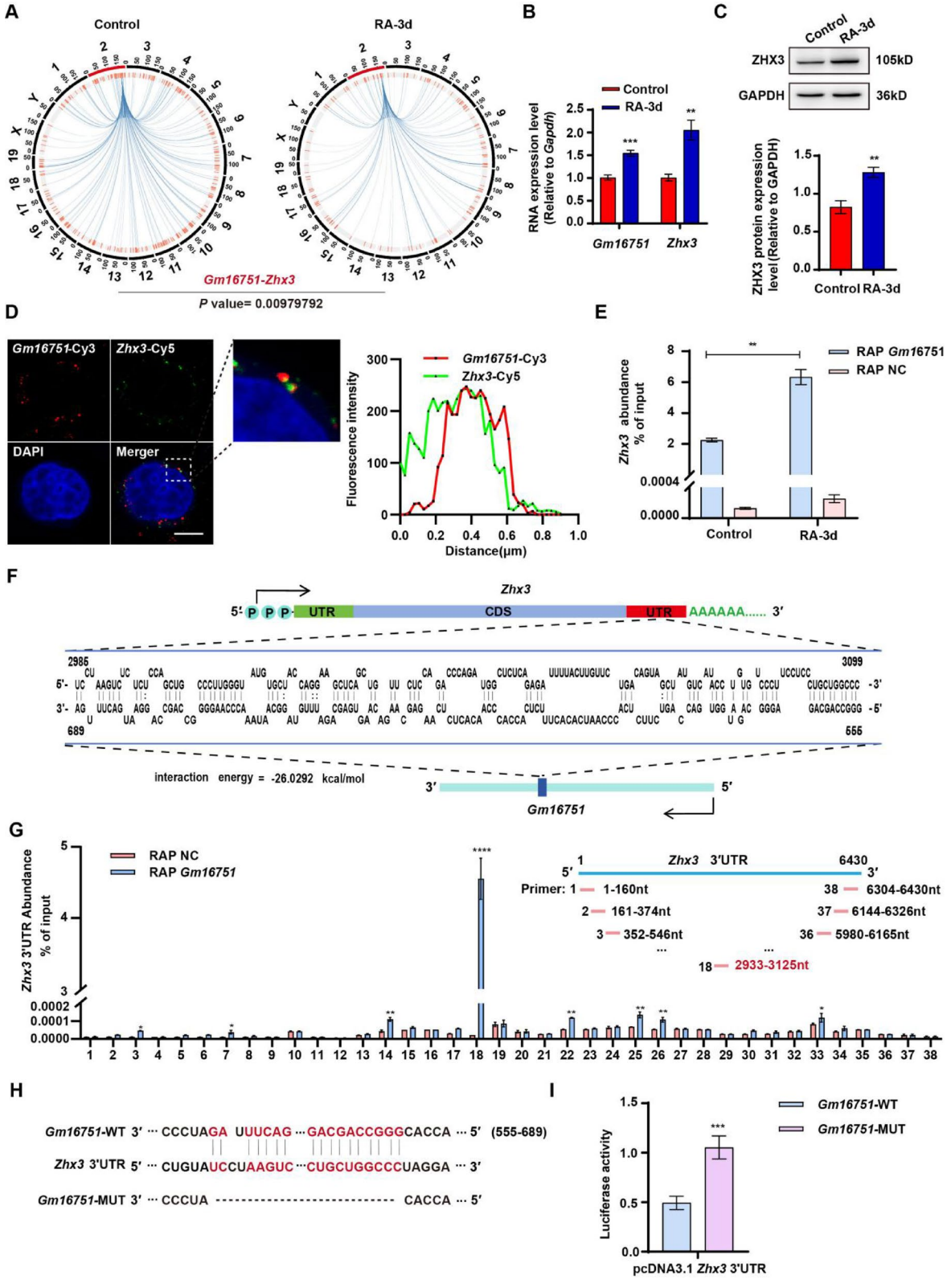

Fig. 2 (See legend on next page.)

(See figure on previous page.)

Fig. 2 lncRNA *Gm16751* physically and functionally interacts with mRNA *Zhx3* during SSC differentiation. **A** Circos plot depicting RNA-RNA interaction networks of *Gm16751* (on chromosome 2, red) in undifferentiated vs. differentiated SSC. Chromosomal locations are annotated in the outer ring, while the inner ring highlights statistically significant interactions after normalization for transcript abundance. Notably, the *Gm16751–Zhx3* interaction was significantly enhanced post-differentiation ($P = 0.0098$). **B** qRT-PCR analysis confirms significant upregulation of *Gm16751* and *Zhx3* transcripts during SSC differentiation. **C** Western blotting validates the differentiation-associated increase in ZHX3 protein levels, consistent with transcriptional data. **D** High-resolution smFISH coupled with confocal microscopy reveals cytoplasmic co-localization of *Gm16751* (red) and *Zhx3* (green) in SSCs. Yellow puncta indicate overlapping foci, with nearest-neighbor distances quantified (lower right). **E** RAP-qPCR using a *Gm16751*-specific antisense probe confirms direct binding to *Zhx3* mRNA, with interaction strength significantly elevated post-differentiation (NC is the *LacZ* biotin probe (used as a negative control)). **F** In silico RNA-RNA interaction model (generated by IntaRNA) predicts interaction region between nucleotides 555–689 of *Gm16751* and the 2958–3099 region of *Zhx3* 3′UTR, suggesting a direct post-transcriptional regulatory mechanism. **G** A segment of the Zhx3 3′UTR (nt 2933–3125) was confirmed as a binding site for the *Gm16751* by RAP-qPCR analysis. Compared to others segment, *Gm16751* binds to *Zhx3* 3′UTR-2933-3125 with high affinity. The upper right part shows a schematic diagram of the primer design, primer sequences in Supplementary Table 7. **H** Schematic illustrating the construction of the *Gm16751* mutant with a deletion of nucleotides 555–689. **I** The wild-type and mutant *Gm16751* sequences were cloned into the pmirGLO luciferase reporter vector and co-transfected with *Zhx3* 3′UTR-2933-3125 (cloned into pcDNA3.1) and pRL-TK vector into 3T3 cells. Luciferase activity was then measured 24 h post-transfection. Data represent mean ± SEM. $n = 3$ independent repeats. Scale bar: 5 μm. Statistical significance: $^{*}P < 0.05$, $^{**}P < 0.01$, $^{***}P < 0.001$, $^{****}P < 0.0001$

interacting partners for *Gm16751* decreased upon differentiation, its binding to *Zhx3* was markedly enhanced ($P = 0.0098$) (Fig. 2A). Three-dimensional genomic interaction map illustrating the spatial proximity of *Gm16751* and *Zhx3* on chromosome 2 (Fig. S3A). And qRT-PCR and Western blotting analysis demonstrated a significant upregulation of both *Gm16751* and *Zhx3* upon SSC differentiation (Fig. 2B, C). To validate this interaction in situ, we performed smFISH, which confirmed robust cytoplasmic co-localization of *Gm16751* and *Zhx3* in SSCs (Fig. 2D). Further evidence was obtained via RAP-qPCR, where an antisense probe targeting *Gm16751* efficiently enriched *Zhx3* transcripts, with binding affinity significantly increasing post-differentiation (Fig. 2E and Fig. S3B). Subsequent IntaRNA-based computational modeling identified a putative binding interface between the 3′UTR of *Zhx3* and *Gm16751* (Fig. 2F), hinting at a possible post-transcriptional regulatory mechanism. We confirmed that *Gm16751* exhibits the most significant enrichment at the *Zhx3* 3′UTR region (nucleotides 2933–3125) using RAP-qPCR (Fig. 2G), which is consistent with the interaction prediction. Additionally, following the deletion of nucleotides 555 to 689 in *Gm16751*(*Gm16751* MUT), the mutant did not exhibit suppressed luciferase activity compared to the wild-type (*Gm16751* WT) (Fig. 2H–I). Collectively, these findings establish a direct interaction between *Gm16751* and *Zhx3*, providing a foundation for future studies on lncRNA-mRNA networks in SSC fate determination.

Gm16751 regulates SSC differentiation by stabilizing *Zhx3* mRNA

To investigate the functional significance of the *Gm16751–Zhx3* interaction in SSC differentiation, we first knocked down *Gm16751* in SSCs using 50 pmol LNA ASOs (Fig. 3A and Fig. S4A). *Gm16751* knockdown significantly reduced both mRNA and protein levels of differentiation markers *Stra8* and *Sycp3* (Fig. 3B-C and Fig. S4B-E). EdU incorporation assays revealed enhanced SSC proliferation upon *Gm16751* knockdown compared to LNA controls (Fig. 3D), while flow cytometry confirmed no induction of apoptosis (Fig. 3E). Consistent with these findings, lentivirus-mediated *Zhx3* knockdown (Fig. 3F-G and Fig. S4F), similarly impaired SSC differentiation (Fig. S4G-H), demonstrating that both molecules are important for SSC development.

Mechanistic studies revealed that *Gm16751* knockdown significantly reduces its enrichment efficiency for *Zhx3*. (Fig. S4I), and decreased ZHX3 protein levels (Fig. 3H). Conversely, *Gm16751* overexpression elevated ZHX3 expression (Fig. S4J-L). Given the cytoplasmic co-localization of *Gm16751* and *Zhx3* observed by smFISH, we hypothesized that *Gm16751* regulates *Zhx3* post-transcriptionally. DRB-mediated transcriptional arrest assays showed accelerated *Zhx3* mRNA decay in *Gm16751*-depleted cells ($t_{1/2}$: 0.78 vs. 1.49 h in controls; Fig. 3I), indicating mRNA destabilization. To examine whether the stability of *Zhx3* depends on the binding sequence of *Gm16751* (nucleotides 555 to 689), we performed RAP-qPCR and stability assays following the overexpression of the *Gm16751* MUT (Fig. 2H and Fig. S4M-N). The results indicated that, compared to the overexpression groups of the *Gm16751* WT and control, the enrichment efficiency of *Zhx3* was significantly reduced in the *Gm16751* MUT (Fig. 3J). More importantly, the stability of *Zhx3* was severely impaired (Fig. 3K). Furthermore, the mutation in *Gm16751* significantly disrupted the differentiation of SSC (Fig. 3L). Furthermore, *Zhx3* overexpression rescued the differentiation defect caused by *Gm16751* knockdown (Fig. S4O-R). These results establish that *Gm16751* maintains *Zhx3* mRNA stability through direct interaction, thereby regulated the differentiation process of SSC.

RPS3 as an RNA-binding protein mediates the in situ interaction between *Gm16751* and *Zhx3*

To identify key RNA-binding proteins (RBPs) associated with *Gm16751*, we performed liquid

chromatography-mass spectrometry (LC-MS) on RAP samples. Comparative analysis revealed 11 significantly enriched and 13 depleted proteins in the *Gm16751* RAP group versus the negative control (NC:*LacZ* biotin probe) (Fig. S5A). Notably, 50% of these proteins localized to the cytoplasm (Fig. S5B), consistent with *Gm16751*'s cytoplasmic distribution. Among the upregulated candidates, ribosomal protein S3 (RPS3) exhibited the most pronounced enrichment (Fig. 4A). Bioinformatic analysis using the RBP2GO database confirmed RPS3's high RBP potential (Fig. S5C). Silver staining of *Gm16751* RAP samples revealed multiple bands, including a prominent ~ 28 kDa band corresponding to RPS3 (Fig. 4B). Subsequent Western blotting further validated RPS3's enrichment in the *Gm16751* RAP group and input samples (Fig. 4C). Structural prediction via AlphaFold3 indicated that RPS3 harbors a KH domain (aa 42–111), a known RNA-binding domain (Fig. 4D). Immunofluorescence confirmed RPS3's cytoplasmic localization in SSC (Fig. 4E). To investigate RPS3's interaction partners, we employed AlphaFold3 to predict binding interfaces between RPS3 and *Gm16751*/*Zhx3*, the RPS3-RNA complex with a predicted local distance difference test (pLDDT) score > 80 (range 0-100), and the predicted template modeling score (pTM) + interface predicted template modeling score (ipTM) > 0.5, indicating moderate reliability in the predicted interface (Fig. S5D-E). These in silico predictions were used solely to guide subsequent experimental validation. RIP-qPCR demonstrated significant co-precipitation of *Gm16751* and *Zhx3* with RPS3 (Fig. 4F-G). CLIP-qPCR was performed to further identify the specific regions of *Gm16751* and *Zhx3* that directly bind to RPS3. We found that the sequences significantly enriched by RPS3 in *Gm16751* and *Zhx3* completely coincide with the regions responsible for the mutual interaction between these two RNAs (Fig. 4H-I and Fig. S5F). This finding not only demonstrates direct binding of RPS3 to these transcripts, but also furthermore indicates that RPS3 acts as an essential molecular scaffold, directly stabilizing the interaction between *Gm16751* and *Zhx3*. In conclusion, our integrative approach identifies RPS3 as a RBP that binds *Gm16751* and interacts with *Zhx3*.

RPS3 regulates SSC differentiation by modulating the *Gm16751–Zhx3* interaction

To elucidate the mechanistic role of RPS3 in SSC differentiation, we performed lentiviral-mediated *Rps3* knockdown (KD) in SSCs (Fig. 5A–C). Strikingly, *Rps3* KD significantly impaired SSC differentiation (Fig. 5D–E), despite endogenous RPS3 protein levels decreasing during normal differentiation (Fig. 5F). We hypothesize that this seemingly contradictory finding may point to a non-standard, ribosome-independent function for RPS3 in regulating spermatogenesis. As RPS3 is a ribosomal small subunit component, we assessed its impact on general protein synthesis using puromycin incorporation assays (5 μg/mL). Under our experimental conditions, no gross reduction in total protein synthesis was detected by puromycin incorporation assay, although subtle changes cannot be ruled out (Fig. 5G), its effect on global protein synthesis was excluded.

Given RPS3's RNA-binding capacity, we hypothesized it mediates the *Gm16751–Zhx3* interaction. RIP-qPCR confirmed reduced *Gm16751* and *Zhx3* enrichment with RPS3 after KD (Fig. 5H). Critically, RAP-qPCR showed their direct interaction was also diminished (Fig. 5I), positioning RPS3 as a bona fide molecular scaffold. Further mechanistic studies revealed that *Zhx3* mRNA stability and protein levels were significantly reduced post-*Rps3* KD, while *Gm16751* remained unchanged (Fig. 5J–L). Neither KD nor overexpression of *Gm16751* altered RPS3 expression (Fig. S6A-D), confirming *Gm16751* as an RPS3 interaction partner rather than a transcriptional target. Taken together, the data indicate that RPS3 acts as a molecular scaffold for the in situ *Gm16751–Zhx3* interaction and affects SSC differentiation through its effects on this interaction and on *Zhx3* stability.

Discussion

Post-transcriptional regulation of SSC differentiation by lncRNA-mRNA interactions

Accumulating evidence underscores the critical role of post-transcriptional regulation, particularly lncRNAs, in mammalian spermatogenesis and SSC differentiation [26–28]. While lncRNAs have been implicated in testicular development, SSC maintenance, and germ cell maturation, the mechanistic basis of lncRNA-mRNA interactions in SSC differentiation remains poorly understood. Our study bridges this gap by elucidating a novel *Gm16751–Zhx3* regulatory axis, demonstrating how their in situ interaction, mediated by RBP RPS3, orchestrates SSC differentiation.

Gm16751: a cytoplasmic lncRNA with differentiation-promoting functions

We identified *Gm16751* as a 1,685-nt differentiation-induced lncRNA localized to the cytoplasm, where it physically interacts with *Zhx3* mRNA. This aligns with emerging paradigms of cytoplasmic lncRNAs, which often regulate mRNA stability, translation, or protein modifications [11, 29]. Unlike nuclear lncRNAs that modulate chromatin dynamics or splicing [11, 29], *Gm16751* exemplifies a cytoplasmic lncRNA that scaffolds RBPs to stabilize target transcripts—a mechanism corroborated by our smFISH and RIC-seq data.

Notably, *Gm16751*'s upregulation during differentiation contrasts with lncRNAs like 033862, which maintain SSC

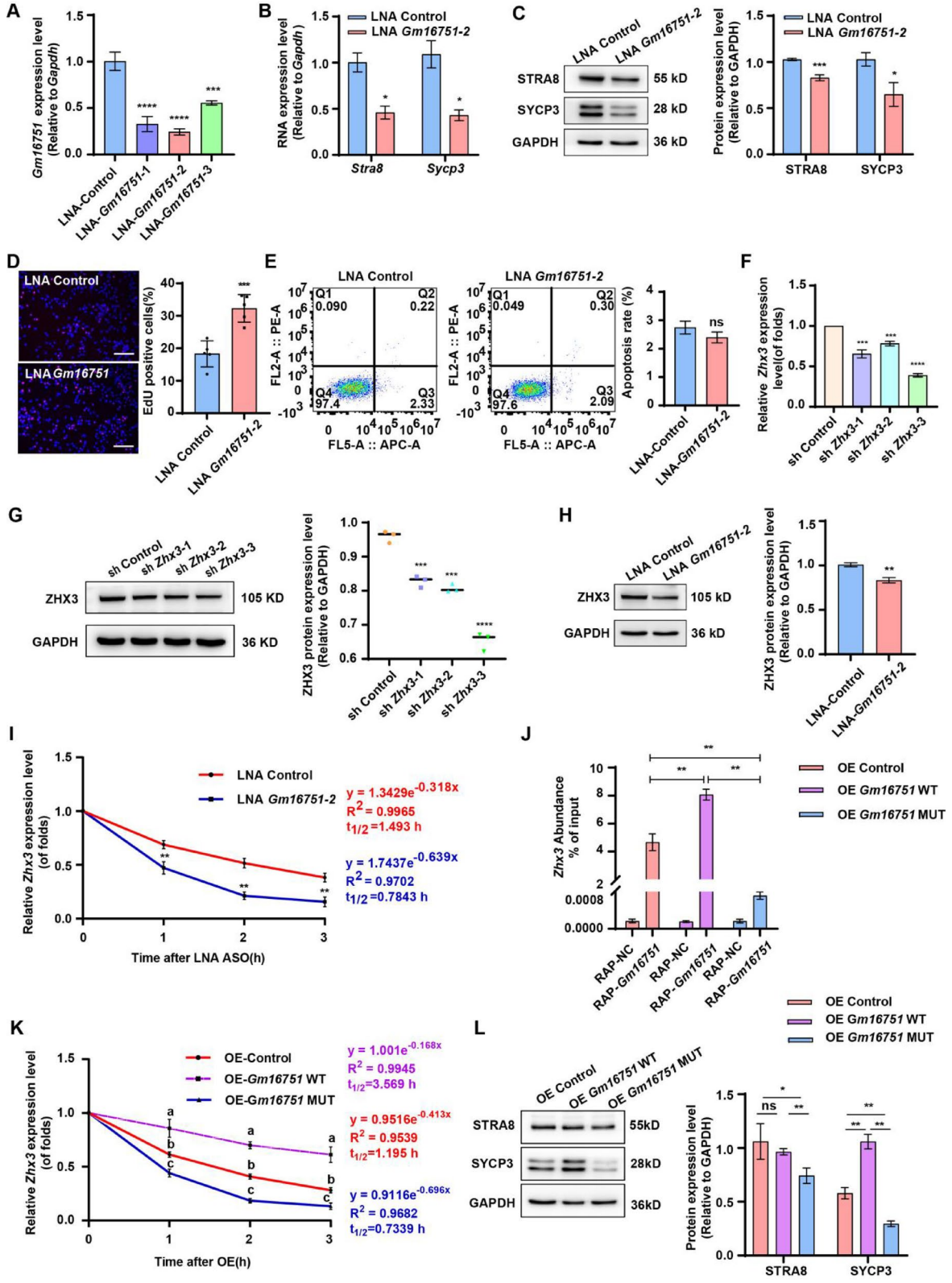

Fig. 3 (See legend on next page.)

(See figure on previous page.)

Fig. 3 The in situ interaction between *Gm16751* and *Zhx3* regulates SSC differentiation. **A** qRT-PCR validation of *Gm16751* KD efficiency (LNA ASO vs. control). **B** qRT-PCR analysis of *Stra8* and *Sycp3* expression following *Gm16751* knockdown during SSC differentiation. **C** Western blotting detection of STRA8 and SYCP3 protein levels post-*Gm16751* knockdown. **D** EdU incorporation assay assessing SSC proliferation after *Gm16751* knockdown. **E** Flow cytometric analysis of apoptosis rates in *Gm16751*-depleted SSC. **F***Zhx3* KD efficiency confirmed by qRT-PCR. **G***Zhx3* KD efficiency confirmed by Western blotting. **H** Western blotting analysis of ZHX3 protein levels after *Gm16751* knockdown. **I***Zhx3* mRNA decay kinetics measured by qRT-PCR after transcriptional inhibition with DRB. Half-life ($t_{1/2}$) values are indicated. **J** RAP-qPCR was used to determine the enrichment efficiency of the *Zhx3* 3′UTR in different groups. **K** Transcriptional inhibition was induced with DRB to assess the decay kinetics of *Zhx3* mRNA across different groups by qRT-PCR and to determine their mRNA half-life ($t_{1/2}$) values. **L** The protein levels of STRA8 and SYCP3 were detected by Western blotting after *Gm16751* mutation. Data represent mean ± SEM. $n = 3$ independent repeats (EdU incorporation assay assessing, $n = 5$ independent repeats). Scale bar: 50 μm. Statistical significance: $^{*}P < 0.05$, $^{**}P < 0.01$, $^{***}P < 0.001$, $^{****}P < 0.0001$; ns: no significance; a, b, c: Different letters signify significant differences

self-renewal via GFRα1 regulation [30]. This dichotomy highlights the functional diversity of lncRNAs in germline development, where spatial expression and interaction partners dictate their roles.

Zhx3: a multifunctional regulator co-opted for spermatogenesis

Zhx3, named zinc fingers and homeoboxes 3, belongs to the ZHX protein family [31]. Beyond its involvement in cancer progression [32], *Zhx3* has emerged as a key regulator of mesenchymal stem cell and osteoblast differentiation [33, 34]. Previous studies have demonstrated that MRG15 deficiency results in the loss of mRNA transcripts from 66 male germ cell-specific genes, including *Zhx3* [35]. Furthermore, *Zhx3* expression was shown to be regulated by microRNAs during spermatogenesis [36]. Our work unveils its necessity for SSC differentiation. The differentiation-coupled upregulation of *Zhx3*, dependent on *Gm16751* as an antisense lncRNA, can bind to the 3′UTR of *Zhx3* and mediated stabilization [37], suggests evolutionary repurposing of this transcriptional regulator for germline development. Prior studies linked *Zhx3* to germ cell biology only indirectly (e.g., via microRNA regulation [36] or MRG15-dependent expression [35]). Our results position *Zhx3* as a direct effector of *Gm16751*, expanding its functional repertoire beyond somatic contexts.

RPS3: a ribosomal protein with non-canonical RBP functions

Similar to many ribosomal proteins, RPS3 participates in diverse cellular processes, such as DNA repair [38, 39], transcription [40], and apoptosis [41]. Although RPS3 is a core ribosomal component [42], as *Rps3* knockdown did not impair global protein synthesis, its functional mechanisms appear to be independent of translational processes [43]. Previous studies have demonstrated that RPS3 partitions into two functionally distinct populations, including its non-canonical functions associated with RNA splicing, trafficking, and stability [44]. These findings clearly demonstrate its non-canonical functions as a ribosomal protein. We identified RPS3 as the RBP bridging *Gm16751* and *Zhx3*. Mechanistically, RPS3 stabilizes *Zhx3* mRNA may via KH domain-mediated interactions. KH domain can bind to the 3′UTR of mRNA regulate embryonic development and cell differentiation [45, 46]. And a paradigm observed in Drosophila, where RPS3 loss causes spermatogenic defects [47]. This echoes recent RNA interaction capture studies identifying RPS3 as a key RBP in mammalian spermatogenesis [48]. Our work mechanistically links RPS3 to lncRNA-driven mRNA stabilization, offering a plausible explanation for its dysregulation in teratospermia.

While this study provides novel insights into lncRNA-mRNA interactions during SSC differentiation, our study has limitation that warrant consideration: Our findings are based on in vitro models, and the biological relevance of the *Gm16751–Zhx3* interaction remains to be verified in animal systems. And, while our data establish the functional importance of nucleotides 555 to 689 in *Gm16751*, the precise structural basis of the *Gm16751–Zhx3* interaction remains incompletely resolved, the broader functional consequences of the *Gm16751–Zhx3*-RPS3 complex with other regulatory pathways remain largely unexplored in the context of SSC differentiation. Additionally, whether *Gm16751* stabilizes *Zhx3* mRNA uniquely through RPS3 or whether redundant/parallel mechanisms exist remains unknown. Our findings do not exclude such possibilities, and further investigation is needed to determine the exclusivity of this regulatory axis.

Conclusions

We propose a tripartite interaction module (Graphical abstract): (1) In situ interaction, *Gm16751* interacts with *Zhx3* in situ during SSC differentiation; (2) Stabilization, the RPS3 as a RBP stabilizes the *Gm16751-Zhx3* interaction, enhances *Zhx3* mRNA stability; (3) Execution, ZHX3 protein promotes differentiation gene programs (e.g., *Stra8*/*Sycp3*). This study provides novel insights into male germ cell development and spermatogenesis by identifying a cytoplasmic lncRNA–mRNA interaction essential for SSC differentiation. It uncovers the non-ribosomal role of RPS3 as an RBP within germ cells. Future research should focus on elucidating the architecture and functional dynamics of the *Gm16751*/RPS3/*Zhx3* ribonucleoprotein complex, determine whether this regulatory axis induces functional

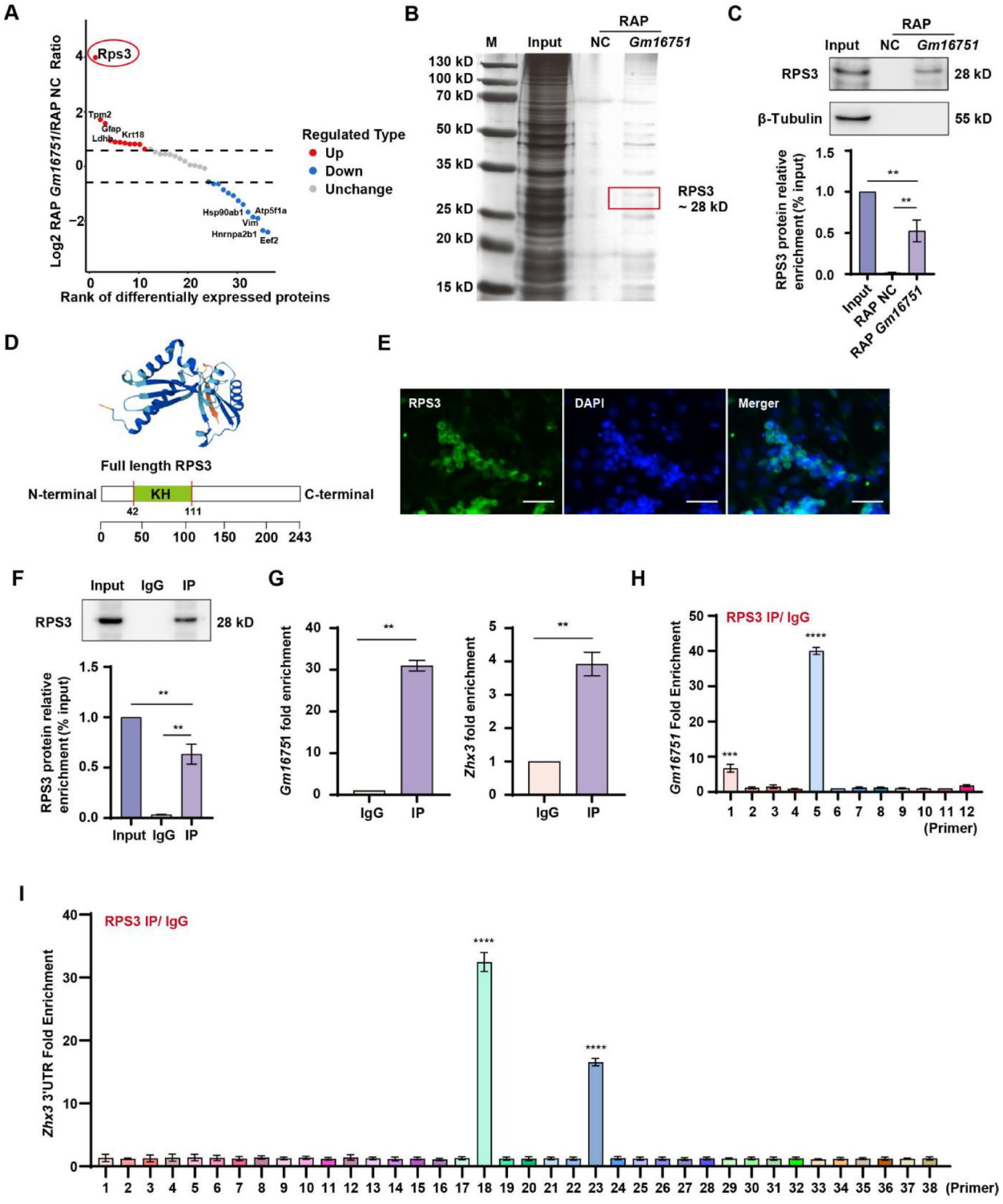

Fig. 4 Identification of RPS3 as an RBP mediating the *Gm16751–Zhx3* interaction. **A** Scatter plot of log2-transformed fold changes (*Gm16751* RAP/NC). RPS3 (highlighted) exhibits the most significant enrichment. **B** Silver-stained SDS-PAGE of RAP samples. A prominent ~ 28 kDa band (arrow) aligns with RPS3's molecular weight. M: Protein marker. **C** Western blotting validation of RPS3 enrichment in *Gm16751* RAP samples. Quantification confirms significant pull-down efficiency versus NC. **D** Predicted 3D structure of RPS3 (AlphaFold3). The KH domain (aa 42–111, magenta) suggests RNA-binding capability. **E** Immunofluorescence staining of SSCs reveals RPS3's cytoplasmic localization. **F** The enrichment efficiency of RPS3 in the RIP assay. **G** RIP-qPCR confirms RPS3's direct binding to *Gm16751* and *Zhx3* transcripts. **H** CLIP-qPCR was performed to identify the specific region within *Gm16751* that directly binds to RPS3. **I** CLIP-qPCR was performed to identify the specific region within *Zhx3* 3'UTR that directly binds to RPS3. The primer sequences in Supplementary Table 7. Data represent mean ± SEM. $n = 3$ independent repeats. Scale bar: 50 μm. Statistical significance: $^{**}P < 0.01$; $^{****}P < 0.0001$

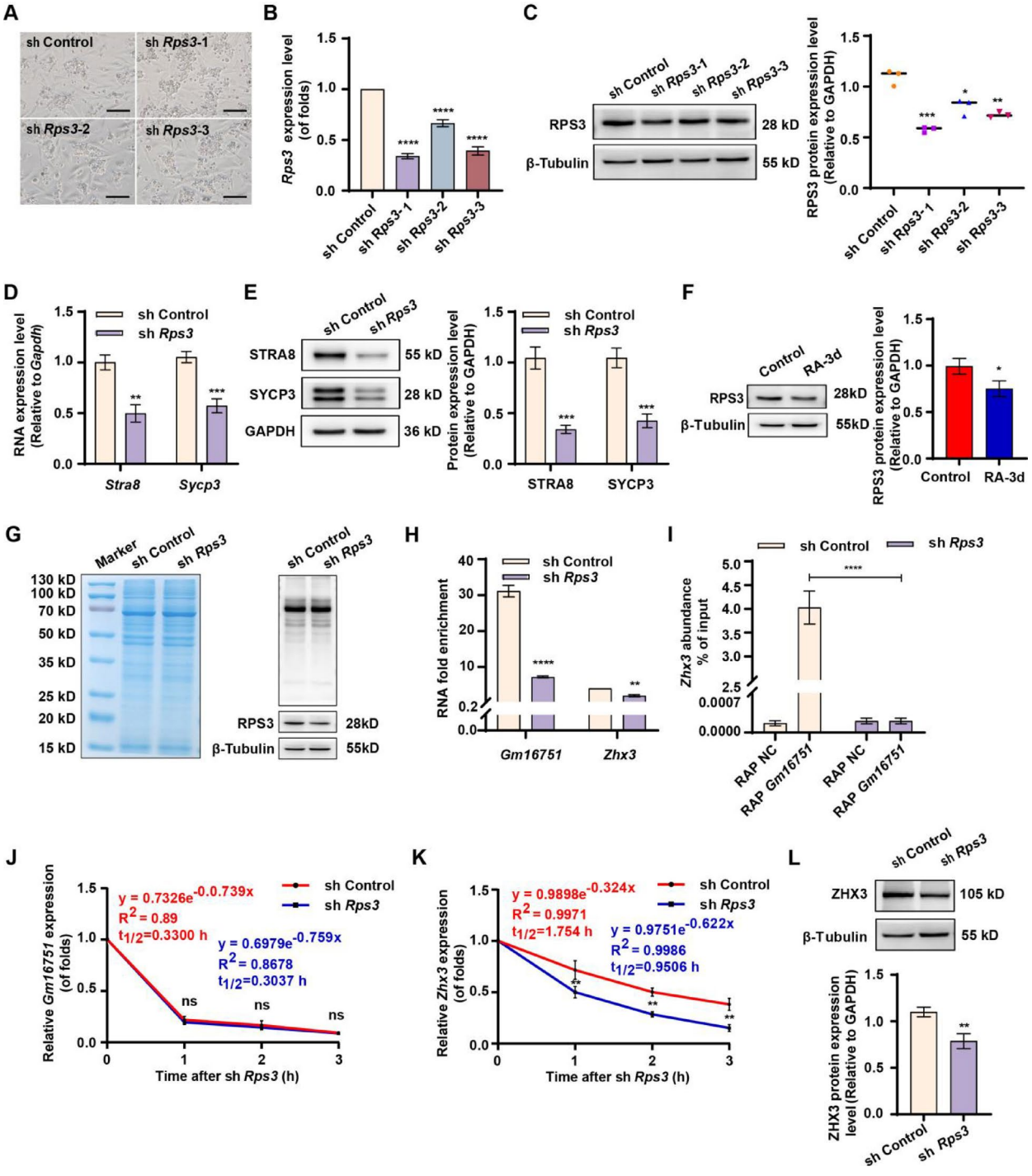

Fig. 5 RPS3 modulates SSC differentiation by regulating the *Gm16751–Zhx3* interaction. **A** Morphological assessment of SSCs following *Rps3* knockdown (KD) (bright-field microscopy). **B** Validation of *Rps3* KD efficiency, qRT-PCR analysis of *Rps3* mRNA levels. **C***Rps3* KD efficiency confirmed by Western blotting. **D** qRT-PCR analysis of *Stra8* and *Sycp3* mRNA levels in SSCs following *Rps3* knockdown (KD) and differentiation induction, demonstrating impaired differentiation. **E** Western blotting validation of STRA8 and SYCP3 protein expression post-*Rps3* KD, corroborating differentiation defects. **F** Endogenous RPS3 protein levels decline during normal SSC differentiation (Western blotting). **G** Global protein synthesis analysis via puromycin incorporation (5 μg/mL, 1 h) and Coomassie staining/Western blotting (anti-puromycin). *Rps3* KD shows no significant translation defects. **H** RIP-qPCR reveals reduced *Gm16751* and *Zhx3* enrichment with RPS3 antibody post-*Rps3* KD. **I** RAP-qPCR confirms diminished *Gm16751–Zhx3* RNA-RNA interaction upon *Rps3* KD. **J** RNA stability assays show *Gm16751* half-life reduction post-*Rps3* KD. **K** RNA stability assays show *Zhx3* mRNA half-life reduction post-*Rps3* KD. **L** ZHX3 protein levels decrease after *Rps3* KD (Western blotting). Data represent mean ± SEM. $n = 3$ independent repeats. Statistical significance: $^{*}P < 0.05$, $^{**}P < 0.01$, $^{***}P < 0.001$, $^{****}P < 0.0001$; ns: no significance

alterations in germ cell development in vivo, and evaluate its potential as a therapeutic target for spermatogenic disorders.

Abbreviations

SSC	Spermatogonial stem cell
RIC	RNA in situ conformation
LncRNA	Long non-coding RNAs
LNA	Locked nucleic acid
ASO	Antisense oligo nucleotides
smFISH	Single-molecule fluorescence in situ hybridization
RAP	RNA antisense purification
RIP	RNA immunoprecipitation
RBP	RNA-binding protein
ZHX3	Zinc fingers and homeoboxes 3
RPS3	Ribosomal protein S3

Supplementary Information

The online version contains supplementary material available at https://doi.org/10.1186/s13578-026-01599-8.

Supplementary Material 1

Supplementary Material 2

Supplementary Material 3

Supplementary Material 4

Supplementary Material 5

Supplementary Material 6

Supplementary Material 7

Supplementary Material 8

Supplementary Material 9

Supplementary Material 10

Supplementary Material 11

Supplementary Material 12

Supplementary Material 13

Acknowledgements

We would like to thank Shanghai Jiao Tong University for providing the experimental platform. We also thank the Laboratory Animal Center of Shanghai Jiao Tong University.

Author contributions

Weijun Gao: performed all experiments unless noted otherwise, analyzed the data, and wrote the manuscript. Bo Xu: performed assistance with the in completing part of the image acquisition. Wenzhi Ma, Xiaojin He: provided guiding suggestions for the writing of this manuscript and performed manuscript review. Ji Wu: performed conceptualization, funding acquisition, supervision, project administration, and manuscript revision.

Funding

This work was supported by the National Key Research and Development Program of China (2022YFA0806301), the Scientific and Technological Innovation Action Program of Shanghai (23JC1402800), and the Shanghai Jiao Tong University 2030 Initiative.

Data availability

The RIC-seq and LongRNA-seq data that support the findings of this study have been deposited in the NCBI Gene Expression Omnibus (GEO) database under accession number GEO: GSE296666, GSE296667. The mass spectrometry proteomics data have been submitted to the ProteomeXchange Consortium and can be accessed via dataset identifiers PXD063805.

Declarations

Ethics approval and consent to participate

All animal procedures were approved by the Shanghai Animal Care and Utilization Committee (approval no. A2023127-001, date: 13 November 2023). The Shanghai Animal Care and Utilization Committee strictly adheres to the principles and guidelines established by the International Council for Laboratory Animal Science (ICLAS).

Competing interests

The authors declare no competing interests.

Author details

[1]School of Basic Medical Sciences, Key Laboratory of Fertility Preservation and Maintenance of Ministry of Education, Ningxia Medical University, Yinchuan 750004, China
[2]Key Laboratory for the Genetics of Development & Neuropsychiatric Disorders (Ministry of Education), Bio-X Institutes, Shanghai Jiao Tong University, Shanghai 200240, China
[3]Department of Obstetrics and Gynecology, Reproductive Medicine Center, Shanghai General Hospital, Shanghai Jiao Tong University School of Medicine, Shanghai 201600, China
[4]HC Key Laboratory of Study on Abnormal Gametes and Reproductive Tract, Anhui Medical University, Hefei 230022, Anhui, China

Received: 25 February 2026 / Accepted: 17 May 2026
Published online: 02 June 2026

References

1. ENCODE Project Consortium. An integrated encyclopedia of DNA elements in the human genome. Nature. 2012;489(7414):57–74.
2. Herman AB, Tsitsipatis D, Gorospe M. Integrated lncRNA function upon genomic and epigenomic regulation. Mol Cell. 2022;82(12):2252–66.
3. Chen L, Kim VN. Small and long non-coding RNAs: past, present, and future. Cell. 2024;187(23):6451–85.
4. Xu Z, Lv C, Gao J, Cui Y, Liu W, He Z, et al. LncRNA ACVR2B-as1 interacts with ALDOA to regulate the self-renewal and apoptosis of human spermatogonial stem cells by controlling glycolysis activity. Cell Mol Life Sci. 2024;81(1):391.
5. Kataruka S, Akhade VS, Kayyar B, Rao MRS. Mrhl long noncoding RNA mediates meiotic commitment of mouse spermatogonial cells by regulating Sox8 expression. Mol Cell Biol. 2017;37(14):e00632.
6. Hu K, Li L, Liao Y, Liang M. LncRNA Gm2044 highly expresses in spermatocyte and inhibits Utf1 translation by interacting with Utf1 mRNA. Genes Genomics. 2018;40(7):781–7.
7. Sunwoo H, Wu JY, Lee JT. The Xist RNA-PRC2 complex at 20-nm resolution reveals a low Xist stoichiometry and suggests a hit-and-run mechanism in mouse cells. Proc Natl Acad Sci U S A. 2015;112(31):E4216–25.
8. Pandya-Jones A, Markaki Y, Serizay J, Chitiashvili T, Mancia Leon WR, Damianov A, et al. A protein assembly mediates Xist localization and gene silencing. Nature. 2020;587(7832):145–51.
9. Green CD, Ma Q, Manske GL, Shami AN, Zheng X, Marini S, et al. A comprehensive roadmap of murine spermatogenesis defined by single-Cell RNA-Seq. Dev Cell. 2018;46(5):651–67.
10. Bridges MC, Daulagala AC, Kourtidis A. LNCcation: lncRNA localization and function. J Cell Biol. 2021;220(2):e202009045.
11. Carlevaro-Fita J, Johnson R. Global positioning system: understanding long noncoding RNAs through subcellular localization. Mol Cell. 2019;73(5):869–83.
12. Koster T, Marondedze C, Meyer K, Staiger D. RNA-binding proteins revisited—the emerging arabidopsis mRNA interactome. Trends Plant Sci. 2017;22(6):512–26.
13. Hung T, Wang Y, Lin MF, Koegel AK, Kotake Y, Grant GD, et al. Extensive and coordinated transcription of noncoding RNAs within cell-cycle promoters. Nat Genet. 2011;43(7):621–9.
14. Schmitt AM, Chang HY. Long noncoding RNAs in cancer pathways. Cancer Cell. 2016;29(4):452–63.
15. Gebauer F, Schwarzl T, Valcarcel J, Hentze MW. RNA-binding proteins in human genetic disease. Nat Rev Genet. 2021;22(3):185–98.
16. Nojima T, Proudfoot NJ. Mechanisms of lncRNA biogenesis as revealed by nascent transcriptomics. Nat Rev Mol Cell Biol. 2022;23(6):389–406.

17. Li K, Zhong S, Luo Y, Zou D, Li M, Li Y, et al. A long noncoding RNA binding to QKI-5 regulates germ cell apoptosis via p38 MAPK signaling pathway. Cell Death Dis. 2019;10(10):699.
18. Zou D, Li K, Su L, Liu J, Lu Y, Huang R, et al. DDX20 is required for cell-cycle reentry of prospermatogonia and establishment of spermatogonial stem cell pool during testicular development in mice. Dev Cell. 2024;59(13):1707–23.
19. Wang P, Wang Q, Chen L, Cao Z, Zhao H, Su R, et al. RNA-binding protein complex AMG-1/SLRP-1 mediates germline development and spermatogenesis by maintaining mitochondrial homeostasis in Caenorhabditis elegans. Sci Bull (Beijing). 2023;68(13):1399–412.
20. Zhao X, Liu L, Huang Z, Zhu F, Zhang H, Zhou D. PTN from Leydig cells activates SDC2 and modulates human spermatogonial stem cell proliferation and survival via GFRA1. Biol Res. 2024;57(1):66.
21. Wen Y, Zhou S, Gui Y, Li Z, Yin L, Xu W, et al. hnRNPU is required for spermatogonial stem cell pool establishment in mice. Cell Rep. 2024;43(4):114113.
22. Cai Z, Cao C, Ji L, Ye R, Wang D, Xia C, et al. RIC-seq for global in situ profiling of RNA-RNA spatial interactions. Nature. 2020;582(7812):432–7.
23. Wang Y, Li X, Gong X, Zhao Y, Wu J. MicroRNA-322 regulates self-renewal of mouse spermatogonial stem cells through Rassf8. Int J Biol Sci. 2019;15(4):857–69.
24. Wang S, Wang X, Ma L, Lin X, Zhang D, Li Z, et al. Retinoic acid is sufficient for the in vitro induction of mouse spermatocytes. Stem Cell Rep. 2016;7(1):80–94.
25. Engreitz JM, Sirokman K, McDonel P, Shishkin AA, Surka C, Russell P, et al. RNA-RNA interactions enable specific targeting of noncoding RNAs to nascent Pre-mRNAs and chromatin sites. Cell. 2014;159(1):188–99.
26. Song X, Kyi-Tha-Thu C, Takizawa T, Naing BT, Takizawa T. 1700108J01Rik and 1700101O22Rik are mouse testis-specific long non-coding RNAs. Histochem Cell Biol. 2018;149(5):517–27.
27. Li L, Wang M, Wang M, Wu X, Geng L, Xue Y, et al. LncRNA analysis of mouse spermatogonial stem cells following glial cell-derived neurotrophic factor treatment. Genom Data. 2015;5:275–8.
28. Sahlu BW, Zhao S, Wang X, Umer S, Zou H, Huang J, et al. Long noncoding RNAs: new insights in modulating mammalian spermatogenesis. J Anim Sci Biotechnol. 2020;11:16.
29. Fazal FM, Han S, Parker KR, Kaewsapsak P, Xu J, Boettiger AN, et al. Atlas of subcellular RNA localization revealed by APEX-Seq. Cell. 2019;178(2):473–90.
30. Li L, Wang M, Wang M, Wu X, Geng L, Xue Y, et al. A long non-coding RNA interacts with Gfra1 and maintains survival of mouse spermatogonial stem cells. Cell Death Dis. 2016;7(3):e2140.
31. Liu Y, Ma D, Ji C. Zinc fingers and homeoboxes family in human diseases. Cancer Gene Ther. 2015;22(5):223–6.
32. Cai Z, Wang S, Zhou H, Cao D. Low expression of ZHX3 is associated with progression and poor prognosis in colorectal cancer. Transl Oncol. 2024;39:101829.
33. Tian Y, Di Y, Bao C, Lin Y, Qin S. [Effect of echinacoside-containing serum in promoting mesenchymal stem cell osteogenic differentiation and ZHX3 expression in rats. Zhongguo Zhong Yao Za Zhi. 2015;40(20):4052–7.
34. Suehiro F, Nishimura M, Kawamoto T, Kanawa M, Yoshizawa Y, Murata H, et al. Impact of zinc fingers and homeoboxes 3 on the regulation of mesenchymal stem cell osteogenic differentiation. Stem Cells Dev. 2011;20(9):1539–47.
35. Iwamori N, Tominaga K, Sato T, Riehle K, Iwamori T, Ohkawa Y, et al. MRG15 is required for pre-mRNA splicing and spermatogenesis. Proc Natl Acad Sci U S A. 2016;113(37):E5408–15.
36. Prados J, Stenz L, Somm E, Stouder C, Dayer A, Paoloni-Giacobino A. Prenatal exposure to DEHP affects spermatogenesis and sperm DNA methylation in a strain-dependent manner. PLoS ONE. 2015;10(7):e132136.
37. Yuan J, Liu X, Wang T, Pan W, Tao Q, Zhou W, et al. The MBNL3 splicing factor promotes hepatocellular carcinoma by increasing PXN expression through the alternative splicing of lncRNA-PXN-AS1. Nat Cell Biol. 2017;19(7):820–32.
38. Park YJ, Kim T, Kim E, Kim HD, Kim J. Ribosomal protein S3 is a novel negative regulator of non-homologous end joining repair of DNA double-strand breaks. FASEB J. 2020;34(6):8102–13.
39. Kim T, Kim HD, Kim J. PKCdelta-dependent functional switch of rpS3 between translation and DNA repair. Biochim Biophys Acta. 2009;1793(2):395–405.
40. Wan F, Anderson DE, Barnitz RA, Snow A, Bidere N, Zheng L, et al. Ribosomal protein S3: a KH domain subunit in NF-kappaB complexes that mediates selective gene regulation. Cell. 2007;131(5):927–39.
41. Kim W, Youn H, Lee S, Kim E, Kim D, Sub Lee J, et al. RNF138-mediated ubiquitination of rpS3 is required for resistance of glioblastoma cells to radiation-induced apoptosis. Exp Mol Med. 2018;50(1):e434.
42. Schafer T, Maco B, Petfalski E, Tollervey D, Bottcher B, Aebi U, et al. Hrr25-dependent phosphorylation state regulates organization of the pre-40S subunit. Nature. 2006;441(7093):651–5.
43. Zhao L, Cao J, Hu K, Wang P, Li G, He X, et al. RNA-binding protein RPS3 contributes to hepatocarcinogenesis by post-transcriptionally up-regulating SIRT1. Nucleic Acids Res. 2019;47(4):2011–28.
44. Watson G, Lester D, Ren H, Forsyth CM, Medina E, Gonzalez Perez D, et al. Fucosylated proteome profiling identifies a fucosylated, non-ribosomal, stress-responsive species of ribosomal protein S3. Cells. 2021;10(6):e1009775.
45. Albarqi MMY, Ryder SP. The endogenous mex-3 3 UTR is required for germline repression and contributes to optimal fecundity in *C. elegans*. PLoS Genet. 2021;17(8):e1009775.
46. Draper BW, Mello CC, Bowerman B, Hardin J, Priess JR. MEX-3 is a KH domain protein that regulates blastomere identity in early *C. elegans* embryos. Cell. 1996;87(2):205–16.
47. Fang Y, Zhang F, Zhan Y, Lu M, Xu D, Wang J, et al. RpS3 is required for spermatogenesis of *Drosophila melanogaster*. Cells. 2023;12(4):573.
48. Li Y, Wang Y, Tan Y, Yue Q, Guo Y, Yan R, et al. The landscape of RNA binding proteins in mammalian spermatogenesis. Science. 2024;386(6720):eadj8172.

Publisher's note